

# Construction of Hyperchaotic Maps Based on 3D-CCC and its Applications in Image Encryption

Jilei Sun<sup>1, \*</sup>

(1. Department of Information Engineering, Shandong University of Aeronautics, BinZhou, 256600, China)

\*Corresponding author: Jilei Sun (e-mail: bzxysjl@163.com)

Funding Information

PhD Scientific Research Foundation of Shandong University of Aeronautics, Award Number: 801003023049

## Abstract

The security performance of chaos-based image encryption algorithms heavily depends on the complexity of the underlying chaotic system. To enhance encryption effectiveness, it is crucial to design chaotic systems with improved dynamic properties.

This paper proposes a novel approach, the 3D Cascaded Cross-Coupling Method (3D-CCC), for constructing 3D hyperchaotic systems by combining three one-dimensional chaotic systems, which can be identical or different. Using this method, we develop a new 3D hyperchaotic map, 3D-ICCCLS, which exhibits superior chaotic characteristics, including good ergodicity, randomness, positive Lyapunov exponents, and high spectral entropy.

Furthermore, we introduce a color image encryption algorithm based on 3D-ICCCLS. The proposed scheme treats the three color channels as an integrated unit, employing cross-channel bit mixing followed by simultaneous permutation and diffusion. This approach achieves a strong encryption effect in a single round. Experimental results demonstrate that the algorithm provides a large key space, high key sensitivity, and strong resistance against common attacks, including brute-force, differential, and noise attacks, ensuring robust security performance.

**Index terms:** hyperchaotic map, image encryption, 3D-CCC, chaos

## 1 Introduction

With the development of information technology and the widespread use of the Internet and mobile Internet, the volume of data transmitted over the network is increasing significantly, with images and videos accounting for a large proportion. At the same time, the number of network information security

incidents and data privacy leaks is also gradually rising, which has attracted the attention of all sectors of society[1][2][3].

Chaotic image encryption has emerged as a pivotal technique in safeguarding digital images[4], leveraging the inherent unpredictability and sensitivity to initial conditions characteristic of chaotic systems. This approach offers a robust framework for securing visual data, addressing the escalating concerns over unauthorized access and distribution in our increasingly digital society. The essence of chaotic image encryption lies in its ability to transform images into forms that are incomprehensible without the correct decryption key, thereby ensuring confidentiality and integrity. This transformation is achieved through algorithms that utilize chaotic maps—mathematical constructs exhibiting deterministic behavior yet appearing random due to their sensitivity to initial conditions. This sensitivity ensures that even minuscule variations in input parameters result in vastly different outputs, making unauthorized decryption exceedingly challenging.

In recent years, chaotic image encryption has emerged as a prominent field of research, leveraging the inherent properties of chaotic systems—such as sensitivity to initial conditions and pseudo-randomness—to enhance the security of image data. Recent advancements in this field have led to the development of innovative encryption algorithms that enhance both security and efficiency.

Shen, Shan, and Tian proposed a novel chaotic image encryption algorithm based on transversals in a Latin square, achieving secure and fast encryption with high information entropy and low correlation coefficients[5]. Similarly, Patidar and Kaur introduced a conservative chaos-driven dynamic DNA coding technique for image encryption, incorporating unique feed-forward and feedback mechanisms to ensure robustness against various cryptanalytic attacks[6]. Additionally, Zhang, Wang, and Liu developed a new chaotic image encryption algorithm combining a 3D chaotic system with a modified version of the AES algorithm, leveraging the high sensitivity of chaotic systems to initial conditions for enhanced security[7]. Furthermore, Li and Zhang presented a chaotic image encryption algorithm utilizing an improved bonobo optimizer and DNA encoding, demonstrating significant improvements in encryption performance[8]. These studies collectively underscore the dynamic nature of chaotic image encryption research and its significance in enhancing data security.

Recent advancements have continued to build upon these foundations. For instance, a comprehensive survey by Wang et al. examined various image encryption algorithms based on chaotic systems, providing an in-depth analysis of their advantages, disadvantages, and potential future research directions[9]. Additionally, a novel algorithm integrating hybrid chaotic maps with DNA coding and substitution boxes was proposed by Zhang and colleagues, demonstrating enhanced security and

efficiency in image encryption processes[10]. Furthermore, a new 3D chaotic system utilizing cellular automata was introduced by Li et al., offering improved performance in image encryption applications[11]. These developments highlight the ongoing evolution and diversification of chaotic image encryption techniques, reflecting their critical role in safeguarding digital visual information.

In the current research on chaotic image encryption, the chaotic systems used are still relatively simple, and the security level is not strong enough. To address these issues, this paper conducts research from two perspectives: the construction of chaotic systems and the design of encryption mechanisms. We propose a method for constructing a hyperchaotic map and a secure and efficient one-round color image encryption algorithm. Firstly, we introduce a 3D cascading crossing coupling (3D-Cascading Crossing Coupling) structure. By utilizing this structure, new 3D hyperchaotic maps can be constructed based on simple one-dimensional chaotic maps. We then build a 3D hyperchaotic map called 3D-ICCCLS based on the 3D-CCC structure. Subsequently, we propose a fast color image encryption algorithm for RGB three-channel mixing encryption based on the 3D-ICCCLS map. This algorithm performs high-low bit cross-mixing on the RGB three channels of the color image and simultaneously carries out permutation and diffusion. It can achieve a good encryption effect in just one round of encryption. Finally, a series of simulation experiments and performance analyses were conducted, which demonstrate that the proposed algorithm has good security performance.

The remainder of the paper is organized as follows: section 2 proposes a 3D cascading crossing coupling (3D-Cascading Crossing Coupling) structure, section 3 create a new 3D chaotic map 3D-ICCCLS and analyze its chaotic behavior, section 4 presents the color image encryption algorithm, section 5 presents the experimental results and security performance analysis, section 6 conclude this paper.

## 2 3D-Cascading Crossing Coupling(3D-CCC) structure

This paper proposes a 3D cascading crossing coupling structure, namely 3D-CCC, which can cascade, cross, and couple three identical or different one-dimensional chaotic maps to construct a new 3D hyperchaotic map. Compared with one-dimensional chaotic maps and two-dimensional hyperchaotic maps, 3D hyperchaotic maps exhibit more complex dynamical behavior and better security. However, their computational complexity is slightly higher, and they take a bit longer to run on a computer. Therefore, when applying them in practice, a trade-off and selection should be made based on the specific requirements and constraints of the scenario. Many existing papers implement chaotic construction through the mod 1 operation[12][13][14][15]. The 3D-CCC method proposed in this paper

does not require the mod 1 operation and has the following advantages.

(1) Better preservation of original chaotic system properties: By using linear mapping, your method avoids the truncation or modification of the value range seen with mod 1, preserving the intrinsic chaotic characteristics of each iterative function.

(2) Simpler expressions: Composing functions with linear mapping avoids the complex expressions introduced by mod 1, resulting in a cleaner and more modular system that is easier to understand and modify.

(3) More rigorous representation: Linear mapping maintains the physical meaning of the function within its original value range, avoiding discontinuities or distortions caused by mod 1, ensuring the system's behavior remains more precise and controllable.

This approach offers greater flexibility and accuracy when designing complex chaotic systems.

To enable different one-dimensional chaotic maps to be cascaded, crossed, and coupled, the output values of the one-dimensional chaotic maps need to be normalized to the same interval (0,1). Generally, let the iteration function value range of a certain chaotic map be the interval (a,b). Since the output of the iteration function in the current round is the input for the next round of iteration, the input range of the iteration function is the same as the output range, which is also (a,b). The output (a,b) can be normalized to the interval (0,1) using equation (1), and the inverse normalization can be performed using equation (2) to restore the values in the (0,1) interval back to (a,b).

$$x_{normalized} = \frac{x - a}{b - a} \quad (1)$$

$$x_{original} = (b - a)x_{normalized} + a \quad (2)$$

Let  $F, G$  and  $H$  be three one-dimensional chaotic maps. Without loss of generality, assume that their input and output intervals are both (0,1). If the intervals are not (0,1), they can be normalized to (0,1) using Equations (1) and (2). The 3D cascading crossing coupling (3D-CCC) is defined as follows:

$$\begin{cases} x_{n+1} = F(x_n G(y_n) + (1 - x_n)H(z_n)) \\ y_{n+1} = F(y_n G(z_n) + (1 - y_n)H(x_{n+1})) \\ z_{n+1} = F(z_n G(x_{n+1}) + (1 - z_n)H(y_{n+1})) \end{cases} \quad (3)$$

In Equation (3),  $x$ ,  $y$ , and  $z$  are the 3D chaotic sequences generated by the 3D-CCC structure.

The structure diagram of the 3D cascading crossing coupling is shown in Figure 1.

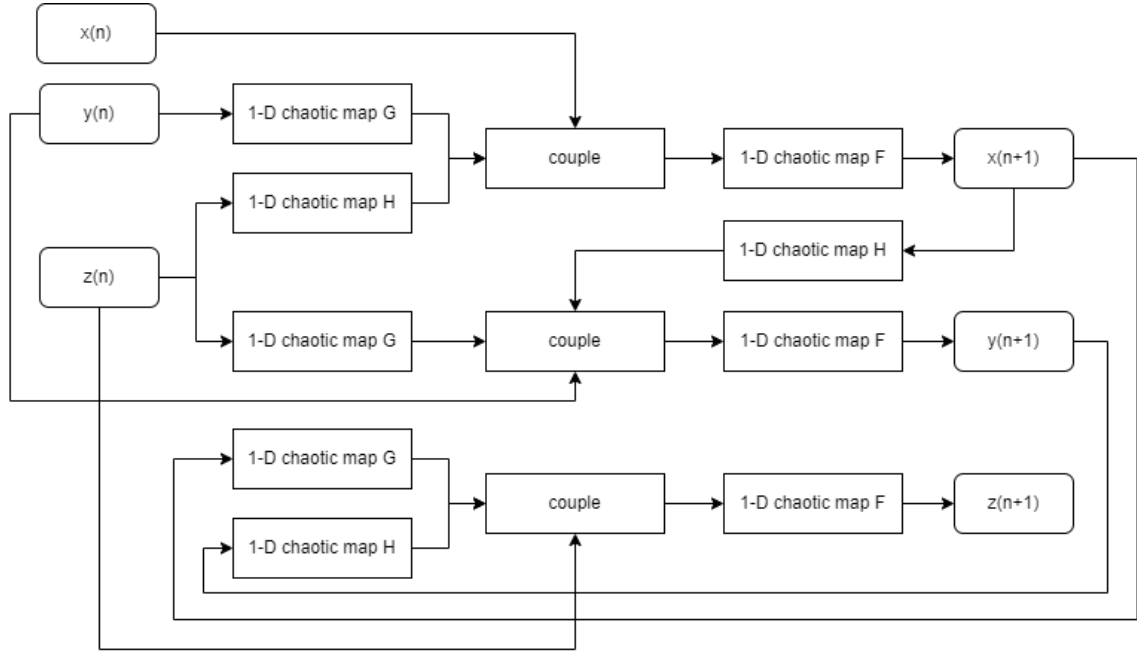


Figure 1. 3D-Cascading Crossing Coupling(3D-CCC) structure

In Figure 1, two one-dimensional chaotic maps  $G(y)$  and  $H(z)$  are first cross-coupled in the proportions of  $x$  and  $1-x$ . The results obtained are then cascaded as inputs into another chaotic map  $F$ , yielding the final output value. By pairwise cross-coupling and cascading the three system variables  $x$ ,  $y$  and  $z$  in this manner, a 3D chaotic map can be constructed.

### 3 3D-ICCCLS Hyperchaotic Map Construction and Analysis

#### 3.1 Construction of 3D-ICCCLS Hyperchaotic Map

In the 3D-CCC structure, by selecting  $F$  as the ICMIC map[16],  $G$  as the Logistic map[17], and  $H$  as the Sine map[18], the 3D-ICCCLS hyperchaotic map can be obtained. When applying the 3D-CCC structure, to facilitate the cascading, modulation, and coupling of different one-dimensional chaotic maps, the inputs and outputs of the one-dimensional chaotic maps are normalized to the interval  $(0,1)$ . The normalized iteration equations for the Sine map, Logistic map, and ICMIC map are given as Equations (4), (5), and (6), respectively.

$$x_{n+1} = \frac{\sin(\mu\pi(2x_n - 1)) + 1}{2} \quad (4)$$

$$x_{n+1} = rx(1 - x_n) \quad (5)$$

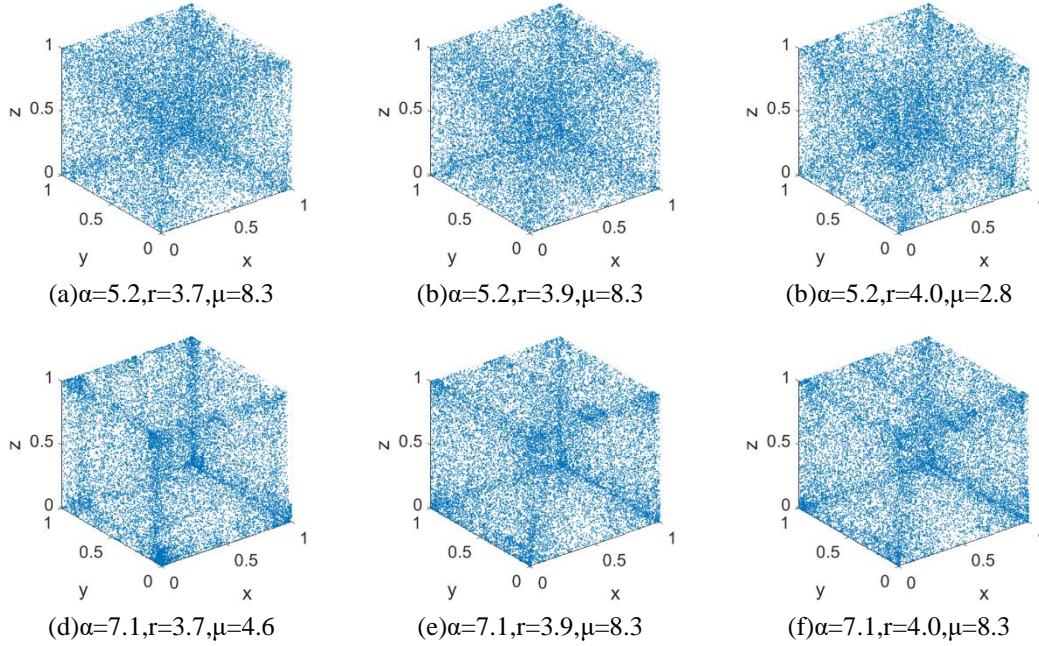
$$x_{n+1} = \frac{\sin\left(\frac{\alpha}{2x_n - 1}\right) + 1}{2} \quad (6)$$

By substituting the above three equations into Equation (3), the iteration equation for the 3D-ICCCLS map can be obtained as follows in Equation (7).

$$\left\{ \begin{array}{l} x_{n+1} = \frac{\sin\left(\frac{\alpha}{2\left(x_n(r y_n(1-y_n)) + (1-x_n)\frac{\sin(\mu\pi(2z_n-1)) + 1}{2}\right) - 1}\right) + 1}{2} \\ y_{n+1} = \frac{\sin\left(\frac{\alpha}{2\left(y_n(r z_n(1-z_n)) + (1-y_n)\frac{\sin(\mu\pi(2x_{n+1}-1)) + 1}{2}\right) - 1}\right) + 1}{2} \\ z_{n+1} = \frac{\sin\left(\frac{\alpha}{2\left(z_n(r x_{n+1}(1-x_{n+1})) + (1-z_n)\frac{\sin(\mu\pi(2y_{n+1}-1)) + 1}{2}\right) - 1}\right) + 1}{2} \end{array} \right. \quad (7)$$

### 3.2 Phase Space Diagram

When the three parameters  $\alpha$ ,  $r$ ,  $\mu$  of the 3D-ICCCLS map take different values, different dynamic behavior characteristics are exhibited. Figure 5.2 shows the phase space diagrams of the 3D-ICCCLS map for certain parameter combinations, with the initial values being  $(x=0.3, y=0.3, z=0.3)$  in all cases.



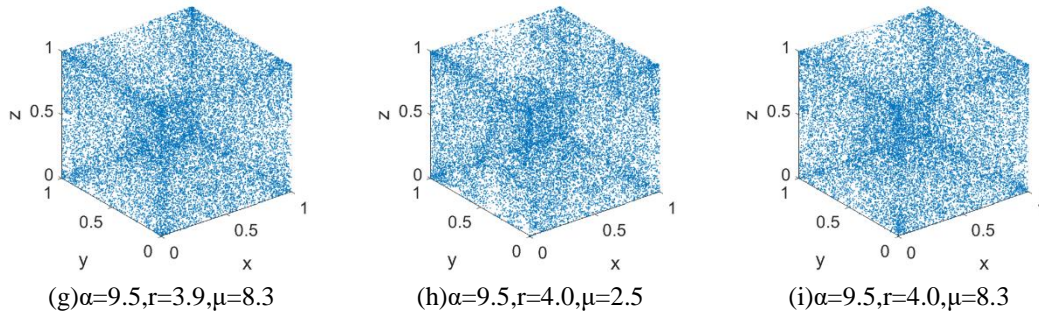


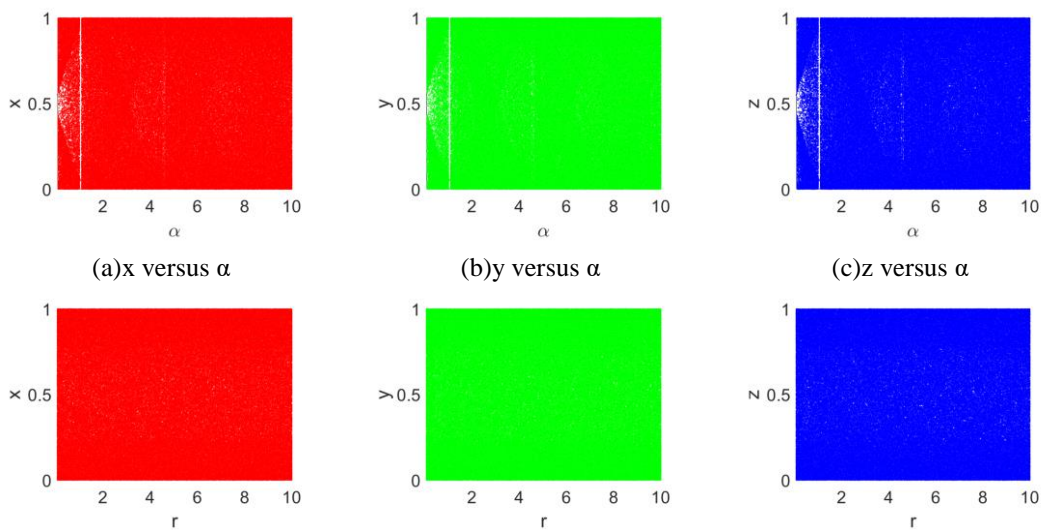
Figure 2. Phase space diagram of 3D-ICCCLS

As can be seen from Figure 2, under the vast majority of parameter combinations, the trajectories of the 3D-ICCCLS map fill the entire 3D unit cube and are distributed relatively uniformly. This indicates that the data generated by this chaotic map possess ergodicity and randomness, making it an excellent chaotic system.

### 3.3 Bifurcation Diagram

The 3D-ICCCLS map has three system variables:  $x, y, z$ , and three control parameters  $\alpha, r, \mu$ . Let the default values of these parameters be  $\alpha=10, r=4, \mu=5$ . For each parameter, while keeping two parameters at their default values, the other one is varied. After iterating 1,000 times, 1,000 sets of values for  $x, y, z$  are obtained. By repeating this process, the values of the variables  $x, y, z$  as the parameters change can be obtained, and a bifurcation diagram can be plotted as shown in Figure 3.

As can be seen from Figure 3, for the 3D-ICCCLS map, except for a few individual parameter values, in the vast majority of cases, the three variables of the system almost fill the entire value range space, and the system exhibits a chaotic state with good ergodicity.



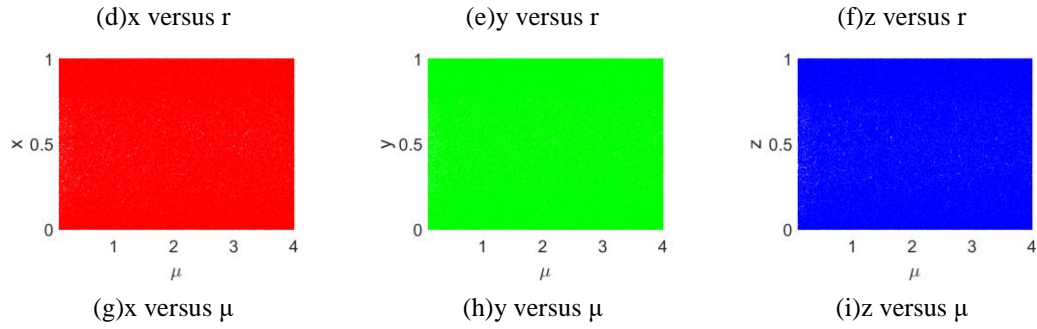
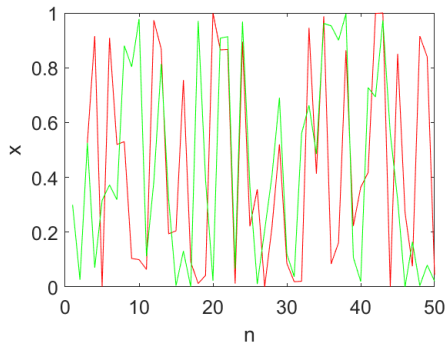


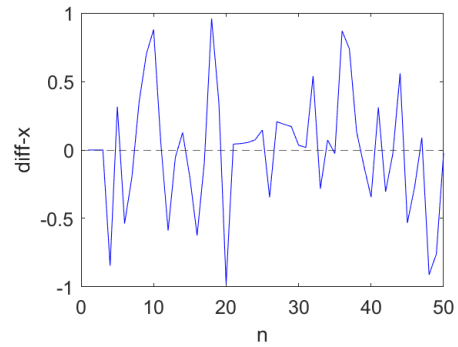
Figure 3. Bifurcation diagram of 3D-ICCCLS

### 3.4 Sensitive Dependency on Initial Values

One characteristic of chaotic systems is their sensitivity to initial conditions. Starting from two adjacent initial points with only a tiny difference, the slight gap in the initial values is continuously amplified as the system iterates, ultimately leading to completely different trajectories. To verify the sensitivity of the 3D-ICCCLS to initial conditions, we set the control parameters  $\alpha=10$ ,  $r=4$ ,  $\mu=5$ . We take two adjacent initial points  $p_0=(x_0, y_0, z_0)$  and  $p_1=(x_0+\delta, y_0+\delta, z_0+\delta)$ , where  $x_0=0.3$ ,  $y_0=0.3$ ,  $z_0=0.3$ ,  $\delta=10^{-16}$ . We iterate each initial point 50 times and plot their  $x$ ,  $y$ ,  $z$  coordinates, as well as the differences in the corresponding coordinates. The results are shown in Figure 4.

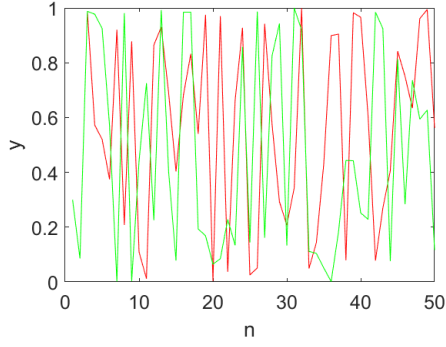


(a) Trajectory of the  $x$ -coordinate of adjacent points

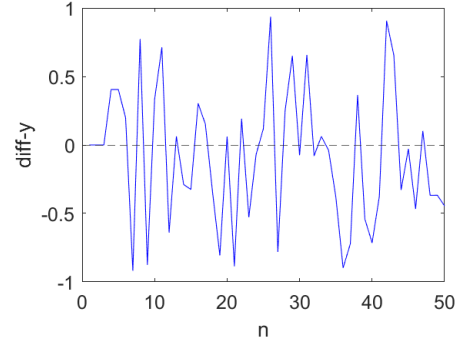


(b) Difference of the  $x$ -coordinate of adjacent points

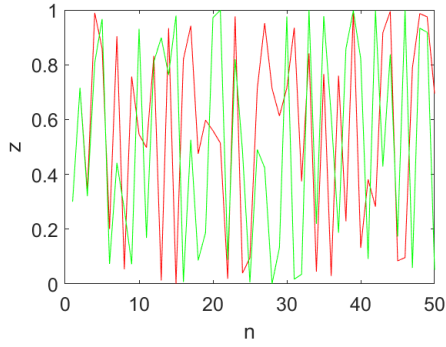




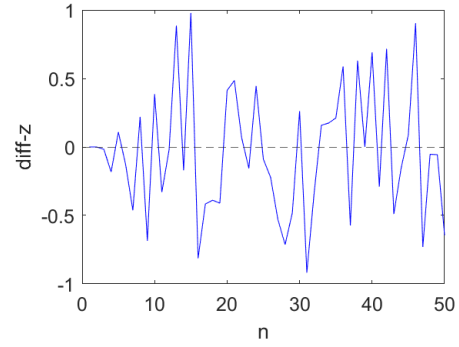
(c) Trajectory of the y-coordinate of adjacent points



(d) Difference of the y-coordinate of adjacent points



(e) Trajectory of the z-coordinate of adjacent points



(f) Difference of the z-coordinate of adjacent points

Figure 4. Sensitive Dependency on Initial Values of 3D-ICCCLS

From parts (a), (c), and (e) of Figure 4, it can be seen that for two very close adjacent points, significant differences appear on all three coordinate axes at the 4th iteration, and from then on, the two trajectories are completely separated. From parts (b), (d), and (f) of Figure 4, the differences in the three coordinates of the adjacent points show an irregular, approximately random distribution. Additionally, the above initial value sensitivity test was conducted on another 1,000 pairs of neighboring points, and the results were similar, indicating that the 3D-ICCCLS has good sensitivity to initial conditions.

### 3.5 Lyapunov Exponents

For the 3D-ICCCLS map, with initial values  $x_0=0.3$ ,  $y_0=0.3$ ,  $z_0=0.3$ , the Lyapunov exponents were calculated, and the results are shown in Figure 5.

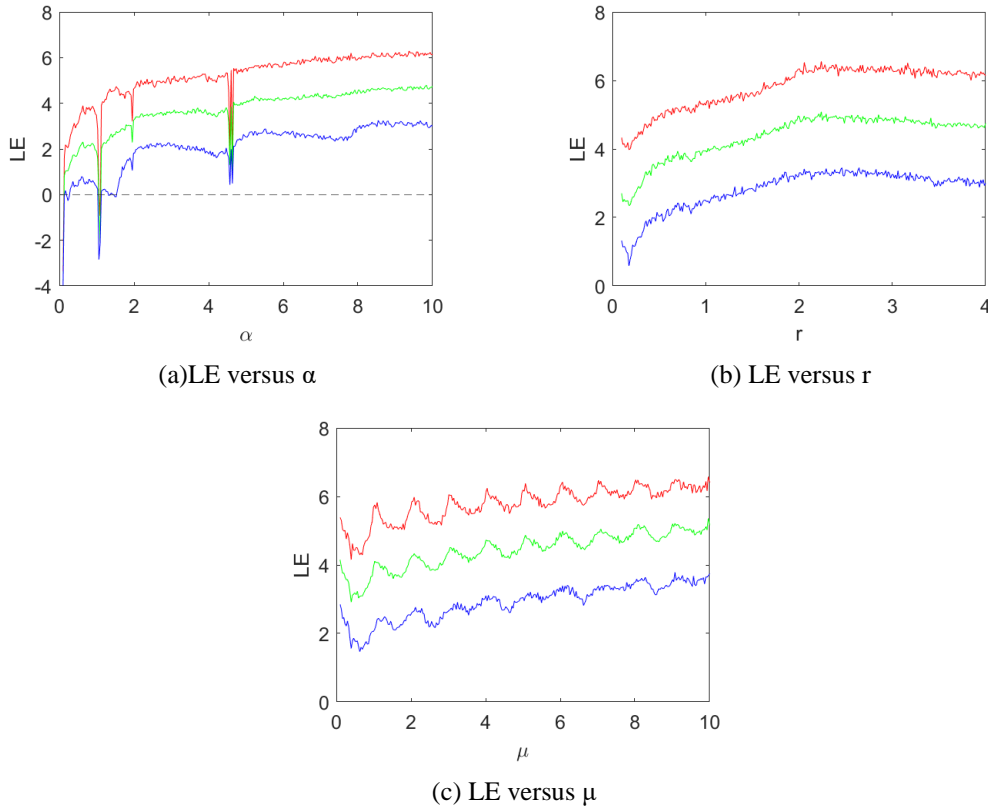


Figure 5. Lyapunov Exponents of 3D-ICCCLS

As can be seen from Figure 5, in the vast majority of the parameter intervals, the 3D- ICCCLS map has three positive Lyapunov exponents, indicating that the system is in a hyperchaotic state. Only within the narrow interval  $\alpha \in [1.03, 1.11]$ , one to three of the Lyapunov exponents are negative. This suggests that the 3D-SCMLI map exhibits a hyperchaotic state for most parameter values and possesses good chaotic properties.

### 3.6 Spectral Entropy

For the 3D-ICCCLS map, with initial values  $x_0=0.3$ ,  $y_0=0.4$ ,  $z_0=0.5$ , and the default values of the three control parameters set as  $\alpha=10$ ,  $r=4$ ,  $\mu=5$ , we generate random sequences by fixing two parameters at their default values and varying the third one each time. We then calculate the average spectral entropy of the three coordinates. The calculation results are shown in Figure 6.

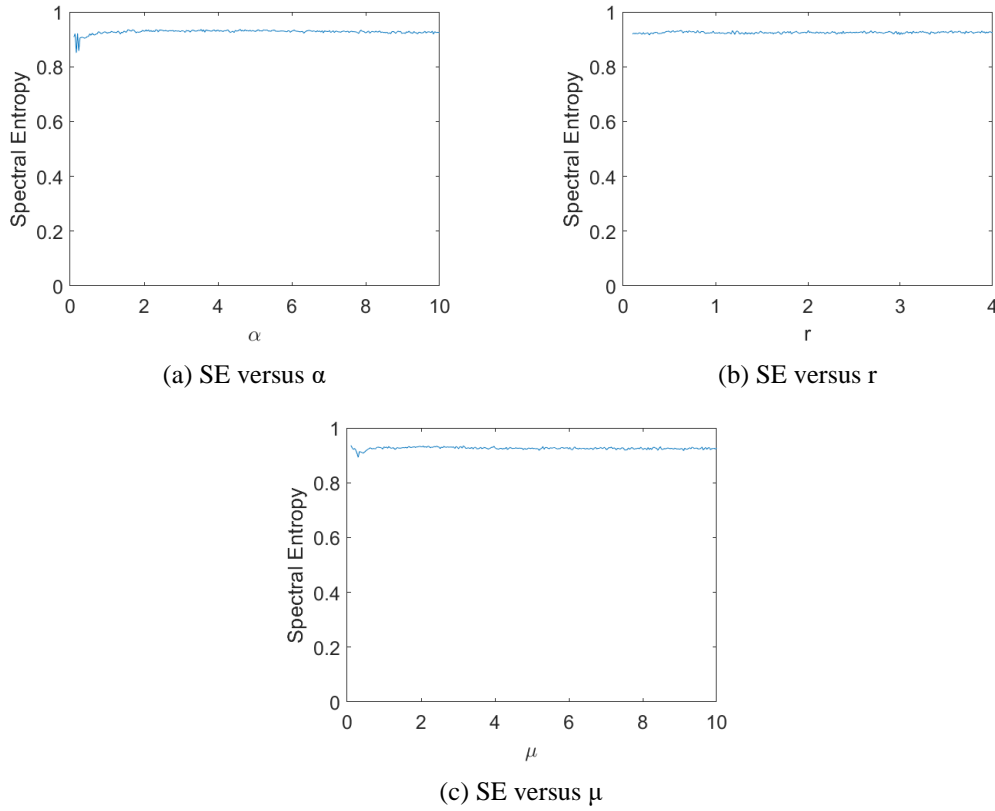


Figure 6. Spectral Entropy of 3D-ICCCLS

As can be seen from Figure 6, the spectral entropy values of the 3D-ICCCLS map fluctuate within the interval  $[0.92, 0.93]$ , indicating that the system has good randomness.

#### 4. RGB Channels Mixing Color Image Encryption Algorithm Based on 3D-ICCCLS

A color image encryption algorithm based on the 3D-ICCCLS hyperchaotic map is proposed, and its overall structure is shown in Figure 7. The algorithm first performs cross channel mixing of the high 4 bits and low 4 bits of the RGB three channels of the plaintext image, and then flattens the mixed image into a one-dimensional pixel vector. Subsequently, keys  $k_1$ - $k_6$  are generated based on the plaintext image and input into the 3D-ICCCLS map to generate chaotic sequences. According to the generated chaotic sequences, the one-dimensional pixel vector is simultaneously permuted and diffused, and then reconstructed into a 3D color image to obtain the cipher image.

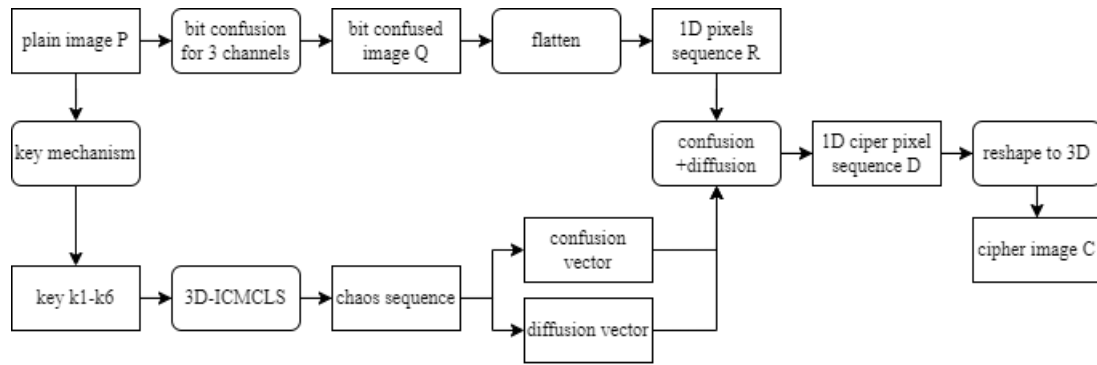


Figure 7. Flow Chart of 3D-ICCCLS Encryption Algorithm

The algorithm has the following characteristics:

- (1) It encrypts the three channels of the color image as a whole, rather than encrypting each channel separately, which increases the complexity of algorithm cracking;
- (2) It confuses the pixels of the three channels at the bit level, eliminating the statistical regularities of the plaintext image pixels;
- (3) It has high encryption efficiency, with pixel permutation and diffusion carried out simultaneously, and only one round of the encryption algorithm is needed to achieve good encryption performance.

#### 4.1 Key Mechanism

The 3D-ICCCLS hyperchaotic map has three control parameters  $\alpha$ ,  $r$ ,  $\mu$ , as well as three initial values  $x_0$ ,  $y_0$ ,  $z_0$ , six parameters as total. The encryption algorithm generates the six required parameters based on the plaintext image. Firstly, a 64-bit hexadecimal Hash string is obtained from the plaintext image. Secondly, 18 decimal integers are generated from the Hash string. Finally, these 18 integers are grouped into sets of three for computation to obtain the six parameters. The key mechanism of the algorithm is shown in Figure 8.

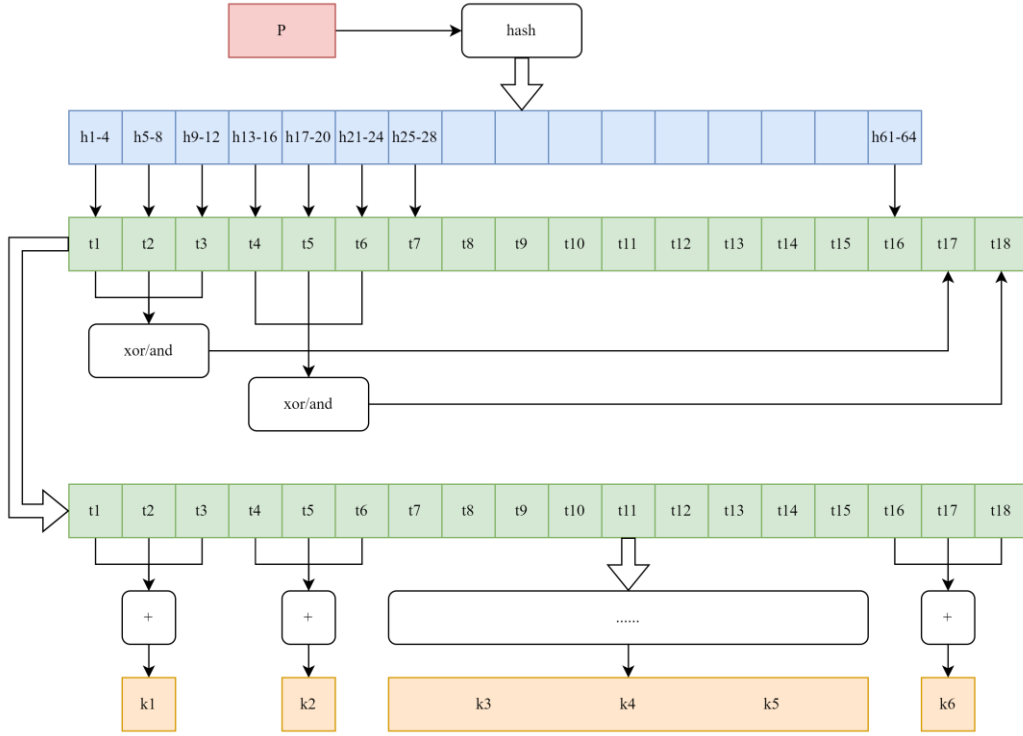


Figure 8. Key mechanism

The details for generating the key are as follows.

**Algorithm1: Key generation**

Input: Plaintext image P.

Output: Six parameters  $k_1$ - $k_6$ .

Step 1: Use a Hash function to generate a 256-bit key from the plaintext image and get 64 hexadecimal characters.

$$h = Hash(P, SHA256) \quad (8)$$

Step 2: Split the 64 hexadecimal characters of h into 16 groups, with each group containing 4 characters, and convert each group into a decimal integer.

$$t(i) = hex2dec(h(4 \times (i - 1) + 1 : 4 \times i)), \quad i = 1, 2, 3, \dots, 16 \quad (9)$$

Step 3: Calculate the values of  $t_{17}$  and  $t_{18}$  according to Equation (10).

$$\begin{aligned} t(17) &= bitxor(bitand(t(1), t(2)), t(3)) \\ t(18) &= bitxor(bitand(t(4), t(5)), t(6)) \end{aligned} \quad (10)$$

Step 4: Divide  $t_1$ - $t_{18}$  into six groups, sum each group to obtain  $k_1$ - $k_6$ , as shown in Equation (11).

$$k(i) = \text{mod} \left( \sum_{j=1}^3 h((i-1) * 3 + j), 2^{16} \right) \quad i = 1, 2, 3, \dots, 6 \quad (11)$$

Step 5: Map  $k_1, k_2, k_3$  to appropriate interval, as shown in Equation (12).

$$\begin{aligned} k(1) &= 3 + 3 \times k(1) \\ k(2) &= 3.7 + 0.3 \times k(2) \\ k(3) &= 5 + 5 \times k(3) \end{aligned} \quad (12)$$

Step 6: Obtain the final  $k_1$ - $k_6$ , which successively represent the three control parameters  $\alpha, r, \mu$ , and the three initial values  $x_0, y_0, z_0$ .

#### 4. 2 Cross Channel Bits Mixing

When encrypting a color image, first perform bit level mixing on the RGB channels of the color image. Split each pixel into the high 4 bits and the low 4 bits, represented by RH, RL, GH, GL, BH, and BL respectively. Then, rearrange and recombine the high and low 4 bits of the RGB three channels to obtain the bit-level mixed image, as shown in Figure 9.

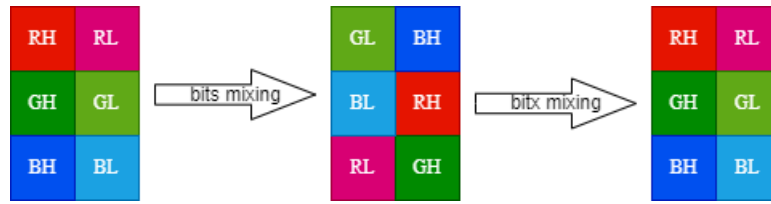


Figure 9. Cross-Channel Bits Mixing

As can be seen from figure 9, performing bits mixing on the original image P yields the mixed image Q, and performing another round of bit mixing on the mixed image Q restores the original image P. This property facilitates the encryption and decryption processes.

#### 4. 3 Confusion and Diffusion

In the encryption process of this algorithm, permutation and diffusion are simultaneously performed, and only one round of encryption can achieve good encryption performance. The detailed process is as follows.

##### **Algorithm 2. Confusion and Diffusion**

Input: color image Q.

Output: cipher image C.

Step 1: Using the 3D-ICCCLS hyperchaotic map to generate a 3D chaotic sequence X, Y, Z of

length  $n$  based on the six parameters (three control parameters  $\alpha, r, \mu$  and three initial values  $x_0, y_0, z_0$  generated by the key mechanism, where  $n$  is the number of pixels in image  $Q$ ).

$$[X, Y, Z] = 3D - ICCCLS(\alpha, r, \mu, x_0, y_0, z_0, n) \quad (13)$$

Step 2: Flatten the 3D chaotic sequences XYZ into a one-dimensional sequence  $U$  of length  $3n$ .

$$U = [X; Y; Z] \quad (14)$$

Step 3: Sort the one-dimensional chaotic sequence  $U$  to obtain the sorting index vector  $W$ , such that the relationship between  $W$  and  $U$  satisfies the following equation.

$$U(W(1)) \leq U(W(2)) \leq U(W(3)) \leq \dots \leq U(W(n)) \quad (15)$$

Taking a sequence of length 10 as an example, Figure 10 illustrates the correspondence between  $U$ ,  $W$ , and  $U(W(i))$ .

$i$	1	2	3	4	5	6	7	8	9	10
$U$	0.7431	0.3922	0.6555	0.1712	0.7060	0.0318	0.2769	0.0462	0.0971	0.8235
$W$	6	8	9	4	7	2	3	5	1	10
$U(W(i))$	0.0318	0.0462	0.0971	0.1712	0.2769	0.3922	0.6555	0.7060	0.7431	0.8235

Figure 10. Sorting vrector generated by 3D-ICCCLS

Step 4: Convert the 1D chaotic sequence  $U$  into an integer sequence  $V$  in the range of 0-255. This is achieved by multiplying  $U$  by 10000 and then performing a bitwise AND with 0xFF, as shown in Equation (16).

$$V = \text{bitand}(U \times 10000, 255) \quad (16)$$

Step 5: Flatten the RGB color image  $Q$  into a 1D pixel sequence  $R$ .

$$R = \text{reshape}(Q, 3n, 1) \quad (17)$$

Take a 3\*2 color image as example, the flattening operation is shown in Figure 5.17.

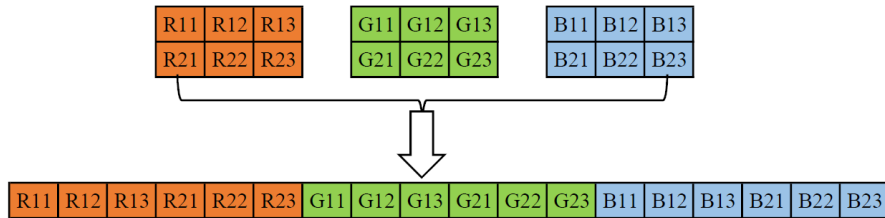


Figure 11. Flatten a RGB color image into a 1D pixel sequence

Step 6: Perform permutation and diffusion on the first pixel of the 1D pixel sequence  $R$ . First, XOR the pixel at position  $W(1)$  with the last two pixels  $R(W(n))$  and  $R(W(n-1))$  in  $R$  and the integer chaotic sequence  $V$ . Then, save the result to the position  $D(1)$ , where  $D$  is the 1D pixel sequence obtained after permutation and diffusion.

$$D(1) = R(W(1)) \oplus R(W(n)) \oplus R(W(n-1)) \oplus V(1) \quad (18)$$

Step 7: Perform permutation and diffusion on the second pixel of the 1D pixel sequence  $R$ . First, XOR the pixel at position  $W(2)$  with  $R(W(n))$  and  $D(1)$ . Then, save the result to the position  $D(2)$ .

$$D(2) = R(W(2)) \oplus D(1) \oplus R(W(n)) \oplus V(2) \quad (19)$$

Step 8: Perform permutation and diffusion on the remaining pixels. The specific operation is to XOR the pixel at position  $W(i)$  with  $D(i-1)$ ,  $D(i-2)$ , and  $V(i)$ , then save the result to the position  $D(i)$ .

$$D(i) = R(W(i)) \oplus D(i-1) \oplus D(i-2) \oplus V(i), \quad i = 3, 4, \dots, n \quad (20)$$

Step 9: Reshape the 1D pixel sequence  $D$  back into a 3D color image structure to obtain the encrypted image  $C$ . Take a  $3 \times 2$  image as example, the process is shown in Figure 12.

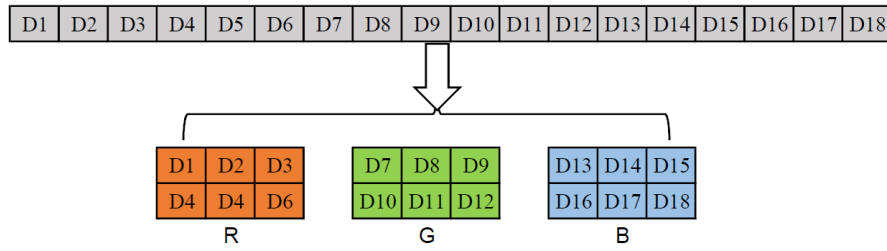


Figure 12. Reshape 1D pixels to 3D image

#### 4.4 Decryption

The decryption algorithm based on 3D-ICCCLS is the inverse operation of the encryption algorithm, and the main steps are described as follows.

##### Algorithm 3: Decryption

Input: cipher image  $C$ , key  $k_1-k_6$ .

Output: plain image  $p$

Step 1: Using the 3D-ICCCLS hyperchaotic map with the keys  $k_1-k_6$  as parameters to generate a 3D chaotic sequence  $X, Y, Z$  of length  $n$ . Then convert it into a 1D sequence  $U$  and generate the integer vector  $V$  and the index vector  $W$ . The progress is the same as in the encryption process.

Step 2: Flatten the ciphertext image  $C$  into a 1D vector  $(D \setminus)$ .



Step 3: Start decryption from the last pixel of D in reverse order until the third pixel from the beginning. This process is the reverse of the encryption process.

$$R(W(i)) = D(i) \oplus D(i-1) \oplus D(i-2) \oplus V(i), \quad i = n, n-1, \dots, 3 \quad (21)$$

Step 4: Decrypt the second pixel of D according to Equation (22).

$$R(W(2)) = D(2) \oplus D(1) \oplus R(W(n)) \oplus V(i) \quad (22)$$

Step 5: Decrypt the first pixel of D according to Equation (23).

$$R(W(1)) = D(1) \oplus R(W(n)) \oplus R(W(n-1)) \oplus V(i) \quad (23)$$

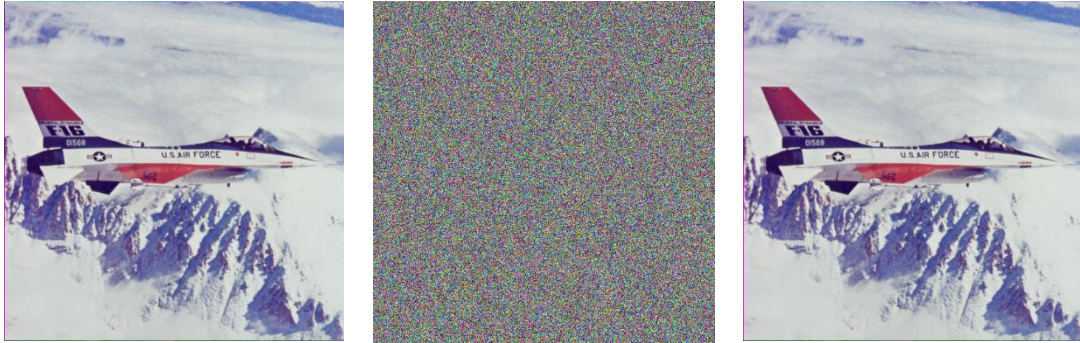
Step 6: Reshape the 1D pixel vector R to a 3D color image Q.

Step 7: Perform bits mixing on Q to obtain the plaintext image P.

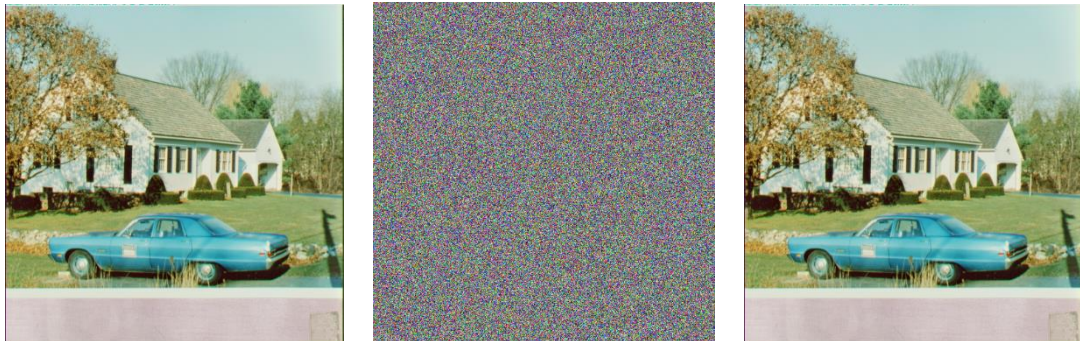
## 5 Simulation Experiment and Performance Analysis

### 5.1 Simulation Result

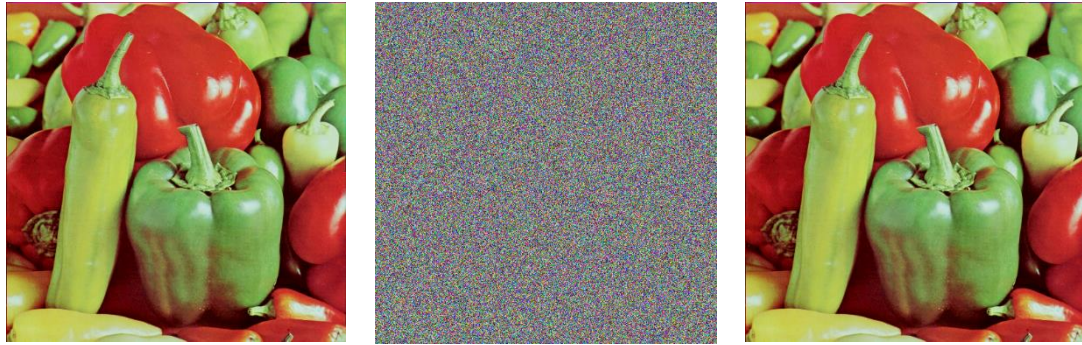
Using the proposed encryption algorithm to encrypt and decrypt three color images: Airplane, House, and Peppers respectively, the experimental results are shown in Figure 13.



(a) Airplane



(b) House



(c)Peppers

Figure 13. Encryption and decryption simulation result

## 5.2 Key Sensitivity

An encryption algorithm should have high sensitivity to keys, a slight change in the key will lead to completely different encryption and decryption results. Specifically, during the encryption process, two different keys (even if they are very similar) will encrypt the same image to produce entirely different cipher images. During the decryption process, only the correct key can decrypt the cipher and obtain the plain image. An incorrect key (even if it is very similar to the correct key) will result in random noise after decryption, revealing no information about the plaintext image.

To analyze the key sensitivity of this algorithm, the following five keys will be used in the experimental process.

K0=26DC1686AA460F215375FE0B468F6F4BD45D067B81BF4BBCF3D73BED5CC1BBD3

K1=26DC1686AA460F215375FE0B468F6F4BD45D067B81BF4BBCF3D73BED5CC1BBD**2**

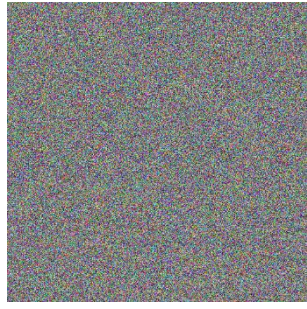
K2=26DC1686AA460F215375FE0B468F6F4BD45D067B81BF4BBCF3D73BED5CC1BB**E**3

K3=26DC1686AA460F215375FE0B468F6F4BD45D067B81BF4BBCF3D73BED5CC1B**A**D3

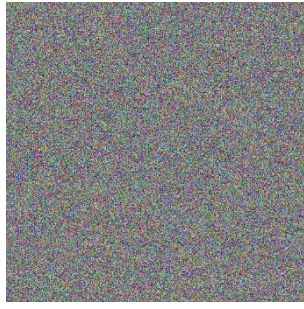
K4=26DC1686AA460F215375FE0B468F6F4BD45D067B81BF4BBCF3D73BED5CC1**C**BD3

The other four keys differ by only one bit from with k0 each (which has been highlighted in bold and red).

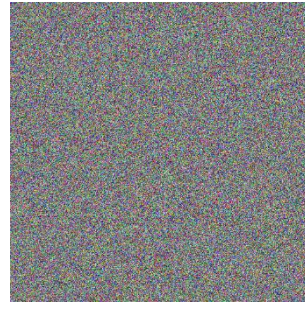
To analyze the key sensitivity in the encryption process of this algorithm, the plaintext image P was encrypted using K0, K1, K2, K3 to obtain the cipher images C0, C1, C2, C3 respectively. Subtract C0 from the other three cipher images and take the absolute value to obtain D1, D2, D3. The results are shown in Figure 14.



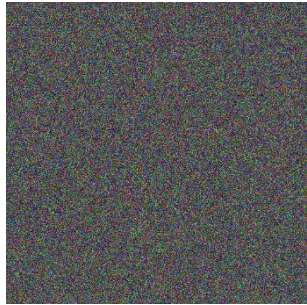
(a) cipher image C1 encrypted  
by K1



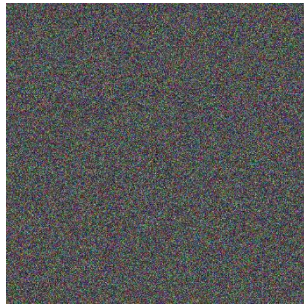
(b) cipher image C2 encrypted  
by K2



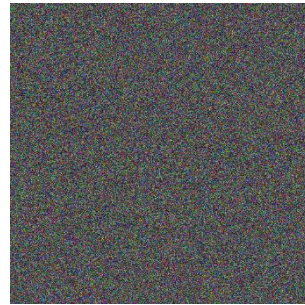
(c) cipher image C3 encrypted  
by K3



(d)  $D1 = \text{abs}(C1 - C0)$



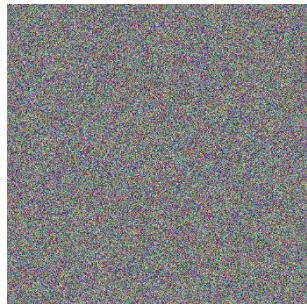
(e)  $D2 = \text{abs}(C2 - C0)$



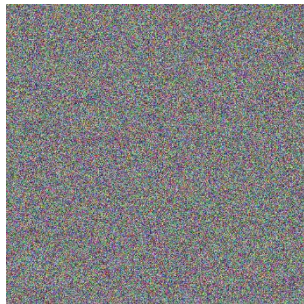
(f)  $D3 = \text{abs}(C3 - C0)$

Figure 14. Key sensitivity in the encryption process

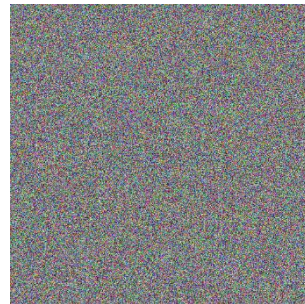
To analyze the key sensitivity in the decryption process of the proposed algorithm, decrypt cipher image C0 with wrong keys K1, K2, K3 to obtain P1, P2, P3 respectively. The images and corresponding histograms are shown in Figure 15.



(a) P1



(b) P2



(c) P3



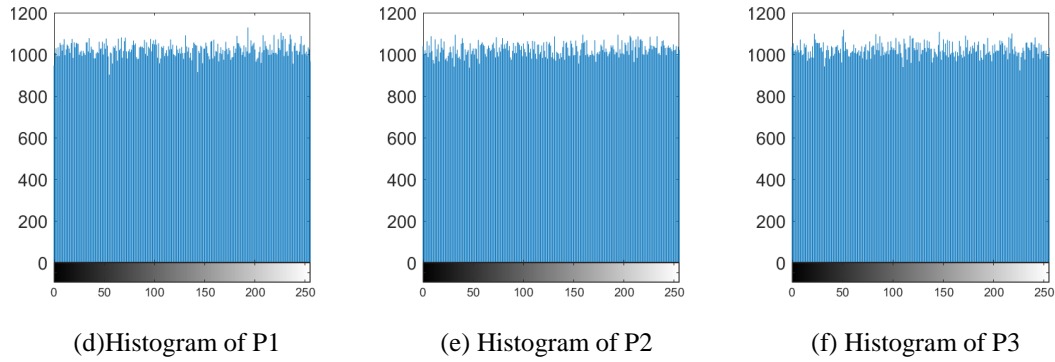


Figure 15. Key sensitivity in the decryption process

As can be seen from Figure 15, only decryption with the correct key can produce the correct plain image. Decryption with an incorrect key results in a meaningless random noise image with an approximately uniformly distribution.

### 5.3 Information Entropy

Information entropy reflects the uncertainty of image information. The higher the entropy value, the more uniformly the image pixel values are distributed, the lower the correlation between pixels, and the more difficult to crack the image. The formula for calculating information entropy is given in Equation (24).

$$H(k) = - \sum_{i=0}^n P(K_i) \log_2 P(K_i) \quad (24)$$

The information entropy of cipher images of the proposed algorithm is calculated and the values are around 7.9993, close to the maximum value of 8, indicating that their pixels are approximately uniformly distributed. A comparison of this algorithm with other algorithms is shown in Table 1.

Table 1 Information entropy analysis

Algorithm	R	G	B	Average
Proposed	7.9993	7.9993	7.9993	7.9993
Ref.[19]	7.9972	7.9972	7.9970	7.9971
Ref.[20]	7.9993	7.9993	7.9993	7.9993
Ref.[21]	7.9991	7.9993	7.9993	7.9992
Ref.[22]	7.9993	7.9992	7.9992	7.9992
Ref.[23]	7.9964	7.9984	7.9961	7.9970

### 5.4 Histogram

Taking the House image as an example, Figure 16 shows the RGB channels histograms of the plain

image and the cipher image encrypted by the proposed algorithm. It can be seen that the plain image pixels exhibit certain regularities in all three RGB channels, with significant differences in the heights of the histograms in different regions. After encryption, the pixel values of the cipher image in all three RGB channels show an approximately uniform distribution, indicating that this algorithm can effectively resist various statistical analysis attacks.

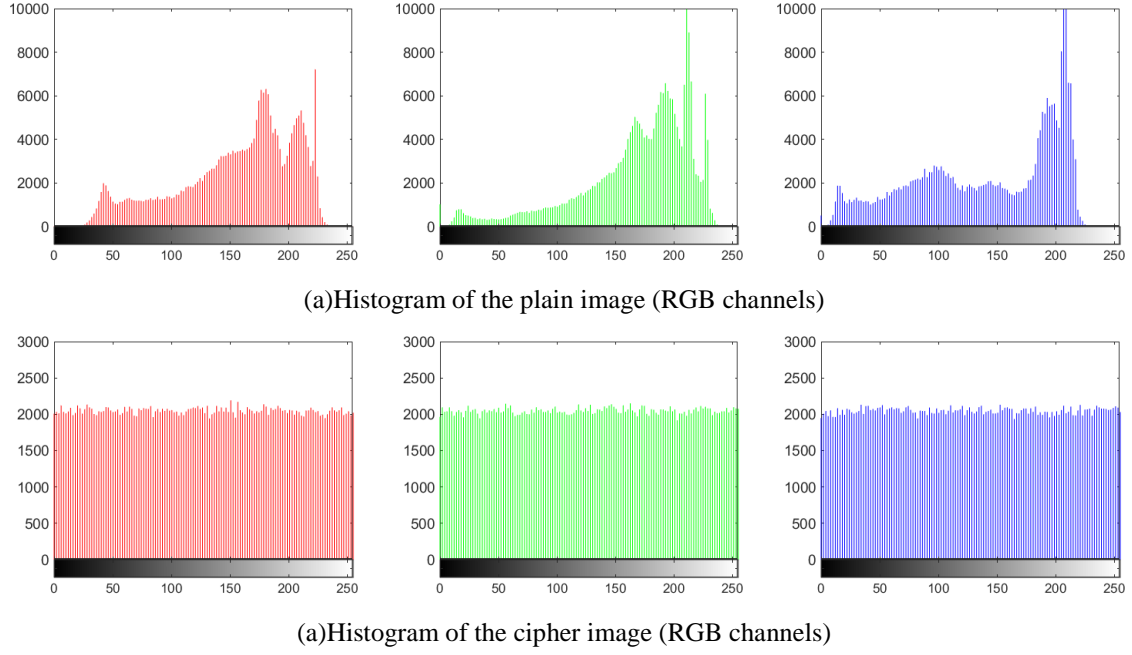


Figure 16. Histogram of the Plain and Cipher Image

## 5.5 Key Space

The key space of an encryption algorithm should be greater than  $2^{100}$  to effectively resist brute-force attacks. In this algorithm, the key consists of six parts: the control parameters  $\alpha$ ,  $r$ ,  $\mu$ , and the system initial values  $x_0$ ,  $y_0$ ,  $z_0$ . All these six values are real numbers, and their value spaces depend on the numerical representation precision of the computer system. In a computer system, for a 64-bit floating-point number, the key space of this algorithm is  $\log_2(10^{3 \times 15} \times 10^{3 \times 16}) \approx 308.9$  bits, much larger than 100 bits. This algorithm can effectively resist brute-force attacks.

A comparison of the key space of the proposed algorithm with other algorithms is shown in Table 2.

Table 2. Key space analysis

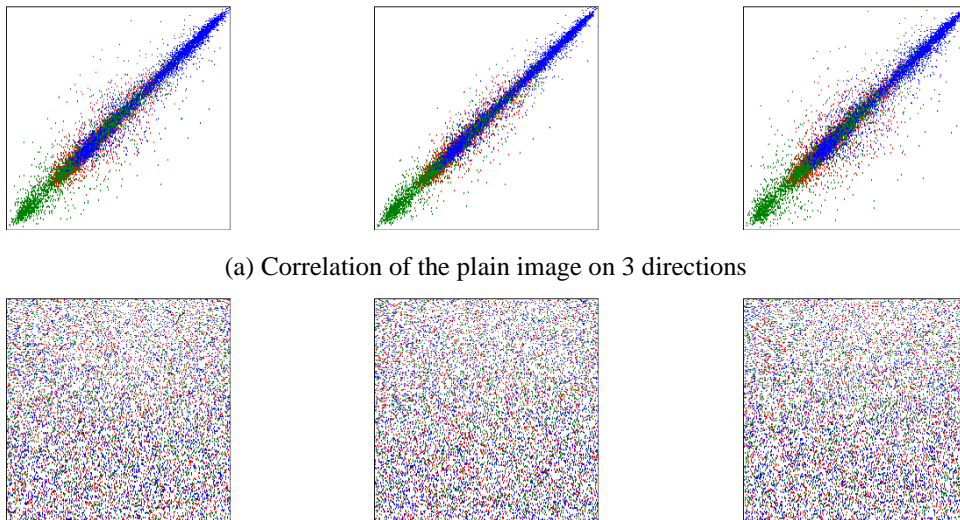
Proposed	Ref.[24]	Ref.[25]	Ref.[26]	Ref.[27]	Ref.[28]
$2^{309}$	$2^{256}$	$2^{256}$	$2^{305}$	$2^{215}$	$2^{287}$

## 5.6 Correlation Analysis

An encryption algorithm should aim to eliminate the correlation between adjacent pixels that exists in the plaintext image to resist correlation analysis attacks. The correlation between adjacent pixels is generally measured in three directions: horizontal, vertical, and diagonal.

Taking the pixel value of a certain pixel  $p_1$  as the x-coordinate and the pixel value of its adjacent pixel  $p_2$  as the y-coordinate, and repeating the sampling  $n$  times, a correlation plot of adjacent pixels with  $n$  points can be drawn. The closer the pixel values of  $p_1$  and  $p_2$ , the more concentrated the plot will be near the diagonal line; the more independent the pixel values of  $p_1$  and  $p_2$ , the more uniformly the plot will be distributed across the entire plane.

To verify the encryption effect of this algorithm, taking the Peppers image as an example, the correlation plots of adjacent pixels in three directions were drawn for both the plaintext and cipher images, as shown in Figures 17. It can be seen that in the plain image, the pixel values of adjacent pixels in the horizontal, vertical, and diagonal directions are very close to each other. In the cipher image, this relationship is completely eliminated, and the pixel values of adjacent pixels show a distribution similar to random.



(a) Correlation of the plain image on 3 directions

(b) Correlation of the cipher image on 3 directions

Figure 17. Correlation of adjacent pixels

To quantitatively measure the correlation between adjacent pixels in an image, the correlation coefficient can be calculated. The closer the correlation coefficient is to 1, the stronger the correlation; the closer it is to 0, the weaker the correlation. A comparison of the adjacent pixel correlation of this

algorithm with several other recent chaotic image encryption algorithms is shown in Table 3. The data indicates that this algorithm has very good encryption effects.

Table 3. Correlation coefficient analysis

Algorithm	Direction	R	G	B
Proposed	H	0.0007	-0.005	0.0005
	V	-0.009	-0.0025	0.0010
	D	0.0028	-0.0031	0.0010
Ref.[29]	-	0.0031	0.0031	0.0031
Ref.[30]	-	-0.0038	-0.0038	-0.0038
Ref.[31]	-	0.0130	0.0141	-0.0258
Ref.[32]	-	0.0012	0.0006	0.0021
Ref.[33]	-	-0.0319	-0.0140	0.0065

## 5.7 Differential Attack

Differential attack is a common cryptographic attack method in which an attacker selects two plain images that differ by only a single pixel, encrypts them, and then analyzes the resulting cipher images to identify potential patterns. A robust encryption algorithm should effectively diffuse minor variations in the plaintext image (such as a single-pixel change) across the entire cipher image, thereby preventing the attacker from discovering any meaningful correlations.

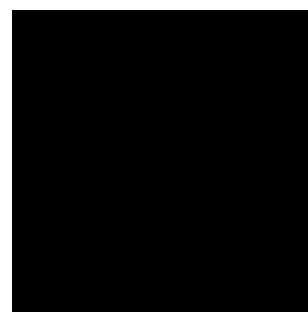
To evaluate the resistance of the proposed encryption algorithm against differential attacks, an experiment was conducted using the Peppers image. A single pixel in the Peppers image was randomly altered to generate a modified image Peppers2. Both Peppers and Peppers2 were then encrypted using the proposed algorithm, producing the corresponding cipher images C1 and C2. To analyze the differences between C1 and C2, their absolute difference image D12 was computed by subtracting C2 from C1 and taking the absolute value. The results of this experiment are presented in Figure 18.



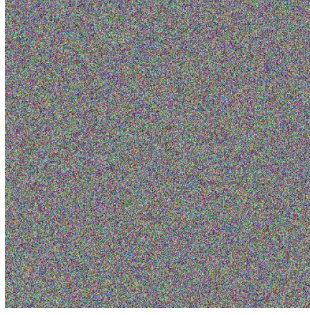
(a) Plain image Peppers



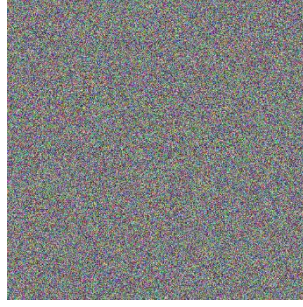
(b) Plain image Peppers2



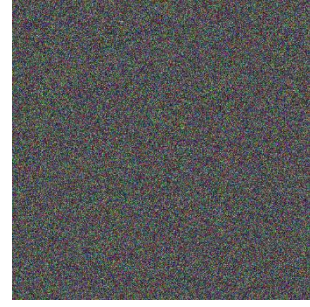
(c)  $\text{abs}(\text{Peppers} - \text{Peppers2})$



(d) C1: Cipher image of Peppers



(e) C2: Cipher image of Peppers2



(f) abs(C1-C2)

Figure 18. Differential attack analysis

The NPCR and UACI metrics can be used to quantitatively measure the extent of pixel changes between two images under differential attack[34]. The NPCR and UACI values of the proposed algorithm were compared with those of other algorithms, and the results are presented in Table 4.

Table 4 Comparison of NPCR and UACI

Algorithm	Proposed	Ref.[35]	Ref.[36]	Ref.[37]	Ref.[38]
NPCR	96.6075	99.6333	99.6124	99.6016	99.5995
UACI	33.4550	33.4395	29.2827	33.4619	33.4480

## 6 Conclusion

In this paper, we proposed a novel method, the 3D Cascaded Cross-Coupling Method (3D-CCC), for constructing hyperchaotic maps from one-dimensional chaotic systems. Using this approach, we developed a new 3D hyperchaotic map, 3D-ICCCLS, which exhibits excellent chaotic properties, including good ergodicity, randomness, positive Lyapunov exponents, and high spectral entropy.

To demonstrate the applicability of 3D-ICCCLS, we designed a color image encryption algorithm that processes RGB channels as an integrated unit. By incorporating cross-channel bit mixing and a simultaneous permutation-diffusion strategy, the proposed algorithm achieves a strong encryption effect in a single round. Experimental results confirm that our approach offers a large key space, high key sensitivity, and robust resistance against common attacks such as brute-force, differential, and noise attacks.

The proposed hyperchaotic system and encryption scheme contribute to the development of more secure and efficient chaos-based cryptographic applications. Future work will explore extending the 3D-CCC framework to higher-dimensional chaotic systems and investigating its applications in other



domains such as secure communications and multimedia protection.

## References

- [1] Singh, Ashish, et al. "Secure smart healthcare framework using lightweight DNA sequence and chaos for mobile-edge computing." *IEEE Internet of Things Journal* 10.6 (2022): 4883-4890.
- [2] Gao, Suo, et al. "A Parallel Color Image Encryption Algorithm Based on a 2D Logistic-Rulkov Neuron Map." *IEEE Internet of Things Journal* (2025).
- [3] Hong, Yan, et al. "A novel approach to visual image encryption: 2D hyperchaos, variable Josephus, and 3D diffusion." *Chinese Physics B* (2025).
- [4] Li, Lizong. "A novel chaotic map application in image encryption algorithm." *Expert Systems with Applications* (2024): 124316.
- [5] Shen, Honglian, Xiuling Shan, and Zihong Tian. "A new chaotic image encryption algorithm based on transversals in a Latin square." *Entropy* 24.11 (2022): 1574.
- [6] Patidar, Vinod, and Gurpreet Kaur. "A novel conservative chaos driven dynamic DNA coding for image encryption." *Frontiers in Applied Mathematics and Statistics* 8 (2022): 1100839.
- [7] Zhang, Y., Wang, X., & Liu, S. "A new chaotic image encryption algorithm combining a 3D chaotic system with a modified version of the AES algorithm." *Multimedia Tools and Applications* 83.5 (2024): 1-20.
- [8] Li, H., & Zhang, J. "Chaotic image encryption algorithm utilizing an improved bonobo optimizer and DNA encoding." *Heliyon* 10.3 (2024): e02456.
- [9] Wang, Xingyuan, et al. "A survey of image encryption algorithms based on chaotic system." *The Visual Computer* 38.11 (2022): 3415-3443.
- [10] Zhang, Liang, et al. "Novel image encryption algorithm utilizing hybrid chaotic maps and DNA coding." *Digital Signal Processing* 125 (2022): 103514.
- [11] Li, Chunhua, et al. "Image encryption algorithm based on a new 3D chaotic system using cellular automata." *Chaos, Solitons & Fractals* 167 (2023): 112960.
- [12] Ding, Dawei, et al. "An n-dimensional polynomial modulo chaotic map with controllable range of Lyapunov exponents and its application in color image encryption." *Chaos, Solitons & Fractals* 185 (2024): 115168.
- [13] Kanwal, Shamsa, et al. "An efficient image encryption algorithm using 3D-cyclic chebyshev map and elliptic curve." *Scientific Reports* 14.1 (2024): 29626.
- [14] Hosny, Khalid M., et al. "Multiple image encryption algorithm using channel randomization and multiple chaotic maps." *Scientific Reports* 14.1 (2024): 30597.
- [15] Xu, Chunyun, et al. "An encryption algorithm for multiple medical images based on a novel chaotic system and an odd-even separation strategy." *Scientific Reports* 15.1 (2025): 2863.
- [16] He, Di, et al. "A chaotic map with infinite collapses." *2000 TENCON proceedings. Intelligent systems and technologies for the new millennium (Cat. No. 00CH37119)*. Vol. 3. IEEE, 2000.
- [17] Phatak, Shashikant C., and S. Suresh Rao. "Logistic map: A possible random-number generator." *Physical review E* 51.4 (1995): 3670.
- [18] Griffin, Jory. "The sine map." Retrieved May 4 (2013): 2018.
- [19] He, Qiji, Peiya Li, and Yanyixiao Wang. "A Color Image Encryption Algorithm Based on

- Compressive Sensing and Block-Based DNA Coding." IEEE Access (2024).
- [20] Wang, Cong, et al. "Color image encryption based on discrete memristor logistic map and DNA encoding." *Integration* 96 (2024): 102138.
  - [21] Zhang, Tian, and Shumei Wang. "Image encryption scheme based on a controlled zigzag transform and bit-level encryption under the quantum walk." *Frontiers in Physics* 10 (2023): 1097754.
  - [22] Liang, Zhongyue, et al. "Color image encryption algorithm based on four-dimensional multi-stable hyper chaotic system and DNA strand displacement." *Journal of Electrical Engineering & Technology* 18.1 (2023): 539-559.
  - [23] Mfungo, Dani Elias, and Xianping Fu. "Fractal-based hybrid cryptosystem: Enhancing image encryption with RSA, homomorphic encryption, and chaotic maps." *Entropy* 25.11 (2023): 1478.
  - [24] Kar M, Kumar A, Nandi D, Mandal M K (2018) Image Encryption using DNA Coding and Hyperchaotic System. *IETE Tec. Rev.* 37:12-23
  - [25] Wang, Xingyuan, and Nana Guan. "2D sine-logistic-tent-coupling map for image encryption." *Journal of Ambient Intelligence and Humanized Computing* 14.10 (2023): 13399-13419.
  - [26] Lu, Qing, Linlan Yu, and Congxu Zhu. "Symmetric image encryption algorithm based on a new product trigonometric chaotic map." *Symmetry* 14.2 (2022): 373.
  - [27] Rani, Narbda, Vinod Mishra, and Suvita Rani Sharma. "Image encryption model based on novel magic square with differential encoding and chaotic map." *Nonlinear Dynamics* 111.3 (2023): 2869-2893.
  - [28] Wen, Heping, et al. "Exploring the future application of UAVs: Face image privacy protection scheme based on chaos and DNA cryptography." *Journal of King Saud University-Computer and Information Sciences* 36.1 (2024): 101871.
  - [29] Lone, Manzoor Ahmad, and Shaima Qureshi. "Encryption scheme for RGB images using chaos and affine hill cipher technique." *Nonlinear Dynamics* 111.6 (2023): 5919-5939.
  - [30] Ahuja, B., & Doriya, R. (2023). A secure algorithm using high-dimensional sine map for color image encryption. *International Journal of Information Technology*, 15(3), 1535–1543.
  - [31] Wang, Xingyuan, et al. "An image encryption scheme using bit-plane cross-diffusion and spatiotemporal chaos system with nonlinear perturbation." *Soft Computing* 27.3 (2023): 1223-1240.
  - [32] Haider, Muhammad Imran, et al. "An Innovative approach towards image encryption by using novel PRNs and S-boxes Modeling techniques." *Mathematics and Computers in Simulation* 209 (2023): 153-168.
  - [33] Ye, Guodong, et al. "Image encryption scheme based on blind signature and an improved Lorenz system." *Expert Systems with Applications* 205 (2022): 117709.
  - [34] Gao, Suo, et al. "Development of a video encryption algorithm for critical areas using 2D extended Schaffer function map and neural networks." *Applied Mathematical Modelling* 134 (2024): 520-537.
  - [35] Zhu, Shuqin, and Congxu Zhu. "A visual security multi-key selection image encryption algorithm based on a new four-dimensional chaos and compressed sensing." *Scientific Reports* 14.1 (2024): 15496.
  - [36] Shakir, Huda Rashid, Sadiq Abdul Aziz Mehdi, and Anwar Abbas Hattab. "Chaotic-DNA system for efficient image encryption." *Bulletin of Electrical Engineering and Informatics* 11.5 (2022):

2645-2656.

- [37] Wang, Hui, et al. "A novel image shift encryption algorithm based on the dynamic Joseph ring problem." *Multimedia Tools and Applications* 82.26 (2023): 39897-39927.
- [38] Biban, Geeta, Renu Chugh, and Anju Panwar. "Image encryption based on 8D hyperchaotic system using Fibonacci Q-Matrix." *Chaos, Solitons & Fractals* 170 (2023): 113396.